Thin Solid Films xxx (xxxx) xxxx

Contents lists available at ScienceDirect

Thin Solid Films

journal homepage: www.elsevier.com/locate/tsf

Influence of two-dimensional oxide nanosheets seed layers on the growth of (100)$BiFeO_3$ thin films synthesized by chemical solution deposition

V. Bouquet[a,*], F. Baudouin[a], V. Demange[a,b], S. Députier[a], S. Ollivier[a], L. Joanny[b], L. Rault[b], A. Fouchet[c], M. Guilloux-Viry[a,b]

[a] Univ Rennes, CNRS, ISCR - UMR 6226, 263 Avenue du Général Leclerc, F-35042 Rennes, France
[b] Univ Rennes, CNRS, ScanMAT - UMS 2001, 263 Avenue du Général Leclerc, F-35042 Rennes, France
[c] NORMANDIE UNIV, ENSICAEN, UNICAEN, CNRS, CRISMAT, 6 Boulevard du Maréchal Juin, F-14050 Caen, France

ARTICLE INFO

Keywords:
Bismuth ferrite
Thin films
Chemical solution deposition
Oxide nanosheets

ABSTRACT

Complex oxide thin films of high quality, such as the multiferroic $BiFeO_3$ (BFO) material, are required for integrated oxides electronics. However, the properties of these materials are strongly dependent on their crystalline orientation and their optimal performances are usually obtained on expensive single-crystal substrates. A lower cost alternative approach is the use of oxide nanosheets seed layers that can be deposited on any substrate, including silicon (Si) used in CMOS technology, for the growth of complex oxides with the desired crystallographic orientation. In this work, BFO films were deposited by chemical solution deposition using polymeric precursor method. First, the optimization of synthesis parameters was performed on amorphous silica and on (100)Si substrates. The structural and microstructural characterizations revealed a polycrystalline growth of the BFO films on both substrates and showed the influence of the synthesis temperature, in particular to obtain the pure perovskite phase. The influence of a two-dimensional nanosheets seed layer was then investigated. $Ca_2Nb_3O_{10}^-$ nanosheets were prepared by the exfoliation process of $HCa_2Nb_3O_{10}$ phase that is obtained by cation exchange of the layered $KCa_2Nb_3O_{10}$ niobate in an acidic solution. The nanosheets were deposited directly on both substrates by Langmuir–Blodgett process, followed by the subsequent deposition of BFO by chemical solution deposition. X-ray diffraction and transmission electronic microscopy experiments showed a highly oriented (100) growth of the BFO thin films confirming the great interest of two-dimensional nanosheets seed layers.

1. Introduction

In microelectronics, the ever decrease of device dimensions, *i.e.* the miniaturization of the electronic elements, arrives at a limit due to intrinsic physical limitations for Si-based electronics. In addition to miniaturization, the integration of multifunctional materials can offer the inclusion of advanced functionalities of the marketed devices. In this context, complex oxides have potential applications due to their wide range of versatile functionalities. However, the properties of these multifunctional materials are strongly dependent on their crystalline orientation. Thus deposition on costly and sized-limited single-crystal substrates is usually required to obtain high performances. For integrated oxide electronic, it is possible to use two-dimensional (2D) oxide nanosheets seed layers that can be deposited on any substrate, including silicon used in CMOS technology, and to grow complex oxides with the desired crystallographic orientation. Highly oriented perovskites ($SrTiO_3$, $Pb(Zr,Ti)O_3$, etc.) and binary oxide films (such as TiO_2, ZnO) have been obtained on glass, silicon or stainless steel substrates using 2D nanosheets seed layers with different crystallographic properties in the 2D network, for example square lattice for $Ca_2Nb_3O_{10}^-$ or hexagonal lattice for $MoO_2^{0.4-}$ [1–6].

Among many functional oxides, multiferroic materials are of first interest thanks to their both ferroelectric and ferromagnetic properties and the possible magnetoelectric coupling. In particular, the $BiFeO_3$ (BFO) material has attracted much attention because of its room temperature multiferroic properties [7]. In fact, this material has a rhombohedral distorted perovskite structure and presents high ferroelectric and magnetic transition temperatures: 1103 K for T_c (Curie temperature) and 643 K for T_N (Néel temperature) in bulk material, respectively. These properties, including magnetoelectric coupling effects, make this material very promising for multifunctional devices in different fields of applications (electronics, spintronics, piezotronics, etc.)

* Corresponding author.
E-mail address: valerie.bouquet@univ-rennes1.fr (V. Bouquet).

https://doi.org/10.1016/j.tsf.2019.137687
Received 26 June 2019; Received in revised form 4 November 2019; Accepted 4 November 2019

[8]. Moreover, it is a non-toxic and lead free material.

Many different deposition methods have been used to grow BFO thin films including pulsed laser deposition [9,10], chemical vapor deposition [11,12], sputtering [13,14] and chemical solution deposition using the sol-gel process [15,16] or the polymeric precursor method [17,18]. The chemical solution deposition (CSD) consists in the deposition of a solution on a substrate, typically by dip or spin coating, followed by subsequent annealing treatments of the wet film in order to crystallize the desired material [19]. The CSD presents various advantages: the possibility of depositing on large area surfaces, a precise control of the stoichiometry, low temperatures of synthesis and the use of simple equipment without vacuum or controlled atmosphere necessity. To prepare the coating solution, the polymeric precursor method, derived from the Pechini process [20], is particularly attractive because it is carried out in aqueous media with the use of relatively cheap precursors [21–23].

In this context, the aim of the present work is to study the growth of BFO thin films by CSD, using polymeric precursor method, on amorphous silica and (100) silicon substrates. In particular the influence of 2D oxide nanosheets seed layers was investigated in order to provide a low-cost route for the integration of oriented BFO thin films which is favorable for high performances in microelectronics. The calcium niobate nanosheet with pseudo-perovskite structure, $Ca_2Nb_3O_{10}^-$, was selected as seed layer to promote the oriented growth of BFO because its crystallographic 2D unit cell is close to that of the perovskite.

2. Experimental details

2.1. Synthesis of BFO films by CSD

The BFO thin films were prepared by CSD using the polymeric precursor method to prepare the coating solution. This method based on the Pechini process [20] consists in preparing a polymeric resin where the metallic ions are uniformly dispersed at the atomic level. This resin is obtained by complexing the metallic cations with citric acid in an aqueous solution. Then the addition of ethylene glycol provokes the polymerization of these metal citrates at a slightly increased temperature. The precursors used in this study were bismuth nitrate $Bi(NO_3)_3{\cdot}5H_2O$, iron nitrate $Fe(NO_3)_3{\cdot}9H_2O$, monohydrated citric acid $C_6H_8O_7{\cdot}H_2O$ and ethylene glycol $C_2H_6O_2$. In a first step, the bismuth and iron solutions were prepared separately. The iron citrate solution was prepared by dissolving citric acid and iron nitrate in water, and ethylene glycol was then added. The bismuth precursor was first dissolved in ethylene glycol in order to avoid the formation of insoluble bismuth oxynitrate and then citric acid was introduced. For each cationic solution of iron and bismuth, the [citric acid:cation] molar ratio was [3:1] and the [citric acid:ethylene glycol] mass ratio was [40:60]. In a second step, the two cationic solutions were mixed in appropriate amounts (Bi:Fe = 1:1) and heated at 90 °C under stirring. An excess of 5% in mass of Bi was added aiming to minimize the bismuth loss during the subsequent thermal treatments [17,18]. Indeed the pure phase could not be obtained without bismuth addition. The viscosity of the obtained polymeric resin was then adjusted to ~ 40 cP by controlling the water content (by addition or evaporation of water) and measured using a Brookfield DVII - Pro-viscometer.

The obtained coating solution was spin coated at 1000 rpm for 3 s followed by a rotational speed at 4000 rpm for 10 s (Spin 150 SPS Europe) on amorphous silica (surface: 10 × 10 mm^2, 0.5 mm thick) and on (100)Si substrates (surface: 10 × 10 mm^2, 0.7 mm thick). The wet films were then submitted to two thermal treatments in air (i) pyrolysis at 400 °C for 3 h to eliminate the organic matter, (ii) calcination in the range 450 °C–600 °C for 2 h in order to determine the optimal temperature of the phase synthesis on both substrates. Two layers of coating solution were deposited for each film. The pyrolysis was carried out after each deposition step, whereas the crystallization treatment was only performed once the 2 layers were deposited. In order to study the influence of a 2D nanosheets seed layer, BFO films (2 layers) were also deposited by CSD on $Ca_2Nb_3O_{10}^-$ nanosheets layers previously deposited on both substrates by Langmuir-Blodgett process.

2.2. Synthesis of nanosheets seed layers by Langmuir–Blodgett process

The synthesis of oxide nanosheets is based on the exfoliation of layered phases [1–6,24]. In this present work, the layered perovskite Dion–Jacobson $KCa_2Nb_3O_{10}$ phase ($P2_1/m$, a = 7.741 Å, b = 7.707 Å, c = 14.859 Å, β = 97.51°, JCPDS card No. 01-075-9853) was first synthesized by solid state reaction at 1100 °C for 10 h from K_2CO_3, Nb_2O_5 and $CaCO_3$ precursors in a molar ratio of 1.35:4:3. The potassium calcium niobate was then protonated by exchange in 6 M HNO_3 for 3 days. During this step, the potassium ions K^+, located between negatively charged perovskite slabs (made of three NbO_6 corner-shared octahedra layers) are exchanged by protons, to form hydrated protonated $HCa_2Nb_3O_{10}{\cdot}1{\bullet}5H_2O$ compound (a = 3.854 Å, c = 16.225 Å, JCPDS card No. 00-39-0915). The protonated phase was then exfoliated by reaction with tetra(n-butyl)ammonium hydroxide (TBAOH) in a molar ratio 1:1 for 14 days. The exfoliated (TBA^+, $Ca_2Nb_3O_{10}^-$) nanosheets thus form a stable aqueous colloidal suspension.

After dilution, the colloidal suspension was deposited on amorphous silica and (100)Si by Langmuir–Blodgett process [25–27] with a KSV NIMA instrument. In this method, the colloidal suspension was placed in a trough. The nanosheets float at the air/water interface due to the moderate amphiphilic role of tetra(n-butyl)ammonium cations. Subsequently, the substrate was immersed vertically in the suspension and two barriers were then moved to compress the air-liquid interface (compression speed of 0.5 $mm.s^{-1}$) until an optimized surface pressure of 15 $mN.m^{-1}$. The substrate was then slowly withdrawn from the dispersion and the obtained nanosheets seed layer was then dried at 110 °C for 1–2 h and treated under UV light for 45 min to remove water and to decompose TBA^+ ions.

2.3. Characterizations

The structural characteristics were investigated by X-ray diffraction (XRD) by using a θ-2θ diffractometer (D8 Advance, BRUKER) with a monochromatized $CuK_{\alpha 1}$ wavelength (λ = 1.54056 Å). The surface and the cross-section of the films were observed at 10 kV by scanning electron microscopy (SEM, JSM 7100F, JEOL) in order to determine their morphology and their thickness. Atomic Force microscopy (AFM) images were performed (NT-MDT NTEGRA) with silicon point probe.

Transmission electron microscopy (TEM) experiments were performed using a LaB_6 Jeol 2100 instrument equipped with an Oxford Aztec 80 mm^2 SDD device for EDXS analysis. Transmission electron brightfield and electron diffraction patterns were recorded using a GATAN Orius SC200D CCD (charge coupled device) camera and high-resolution images were recorded using a GATAN US 1000XP camera. Plane-view film samples were obtained by scratching the thin film from the substrate with a diamond tip and by collecting the obtained fragments on an amorphous carbon copper grid (Agar). Cross-section samples were obtained by cutting thin films samples into slabs of ~ 0.5 × 1.8 mm. Two slabs were glued together with film sides facing each other, then thinned by using diamond-lapping films, followed by dimpling with diamond pastes and Ar-milling in a 1010 Fischione instrument.

3. Results and discussion

3.1. BFO thin films grown on amorphous silica and (100)Si

Fig. 1a and 1b show the XRD patterns obtained for BFO films deposited on amorphous silica and (100)Si, respectively, and heat-treated at different temperatures. The pure BFO phase was obtained for all the synthesis temperatures on both substrates except for 600 °C where some

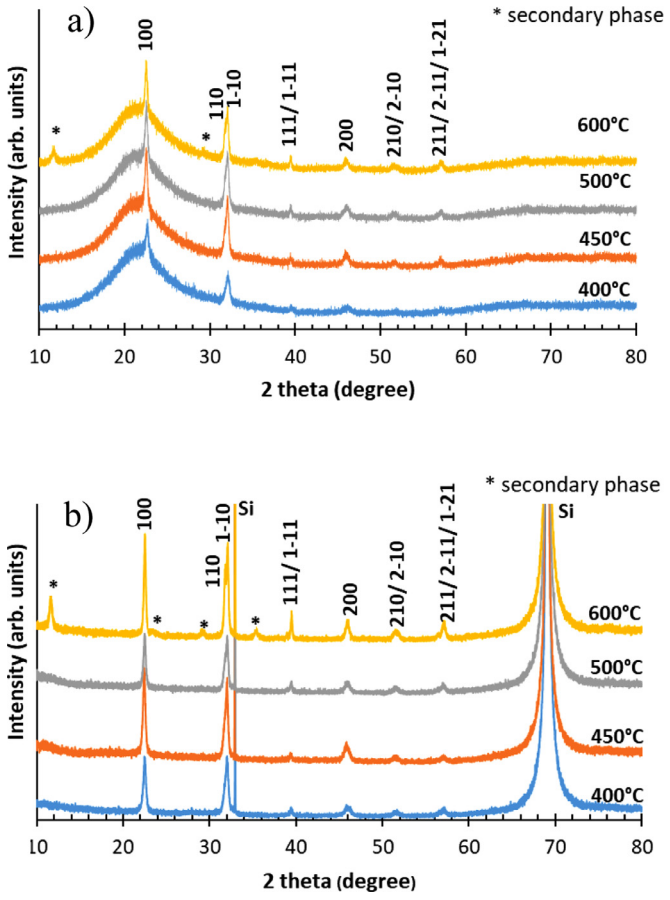

Fig 1. XRD patterns of BFO thin films deposited on silica (a) and on (100)Si (b) and heat-treated at different temperatures.

additional peaks of weak intensity were observed. Many authors have reported the presence of secondary phases such as Bi_2O_3, $Bi_2Fe_4O_9$ or iron oxides in BFO thin films synthesized by different methods and often deposited on Pt/Ti/SiO_2/ Si substrates [9,10,15,17,18]. The presence of these phases mainly depends on the deposition or heat treatment temperatures of the films. However, F. Tyholdt et al. have reported the possible presence of Bi_2SiO_5 phase for a BFO film deposited on glass substrate by CSD and treated at 600 °C [15]. In this present work, the additional peaks of weak intensity at $2\theta = 11.6°$, 23.3°and 35.3° observed at 600 °C can be ascribed to the (200), (400) and (600) reflections of Bi_2SiO_5, respectively ($Cmc2_1$, $a = 15.217$ Å, $b = 5.477$ Å and $c = 5.325$ Å, JCPDS card No. 00-036-0287). The small extra peak at $2\theta = 29.2°$ can be attributed to the main peak of the bulk Bi_2SiO_5 phase, *i.e.* the (311) reflection. The formation of the (100) highly oriented Bi_2SiO_5 is probably due to a reaction of BFO with the substrate at 600 °C.

For all samples, the BFO peaks were indexed in the rhombohedral structure ($R3m$, $a = 3.962$ Å, $\alpha = 89.40°$, JCPDS card No. 01-074-2016) and as expected, no preferential orientation was observed on both substrates (polycrystalline films). Indeed, random orientation of BFO is not surprising on amorphous substrate such as silica, and on silicon (cubic structure, $a = 5.430$ Å, JCPDS No. 00-27-1402) due to the incompatibility between their respective crystalline structure and the presence of amorphous SiO_2 on the substrate surface which is not removed with CSD method.

The SEM and AFM images of the films obtained at 500 °C on silica and on (100)Si are displayed in Fig. 2. The films are crack-free and homogeneous on both substrates and present similar microstructures (Fig. 2a,b) with a uniform grain size around 80 nm (Fig. 2c,d). No significant change of the microstructure was observed in SEM images as a function of heat treatment temperature (not shown here). The films have a thickness around 200 nm and 150 nm on silica and (100)Si respectively, as observed on the SEM cross-sectional views (insets Fig. 2a,b).

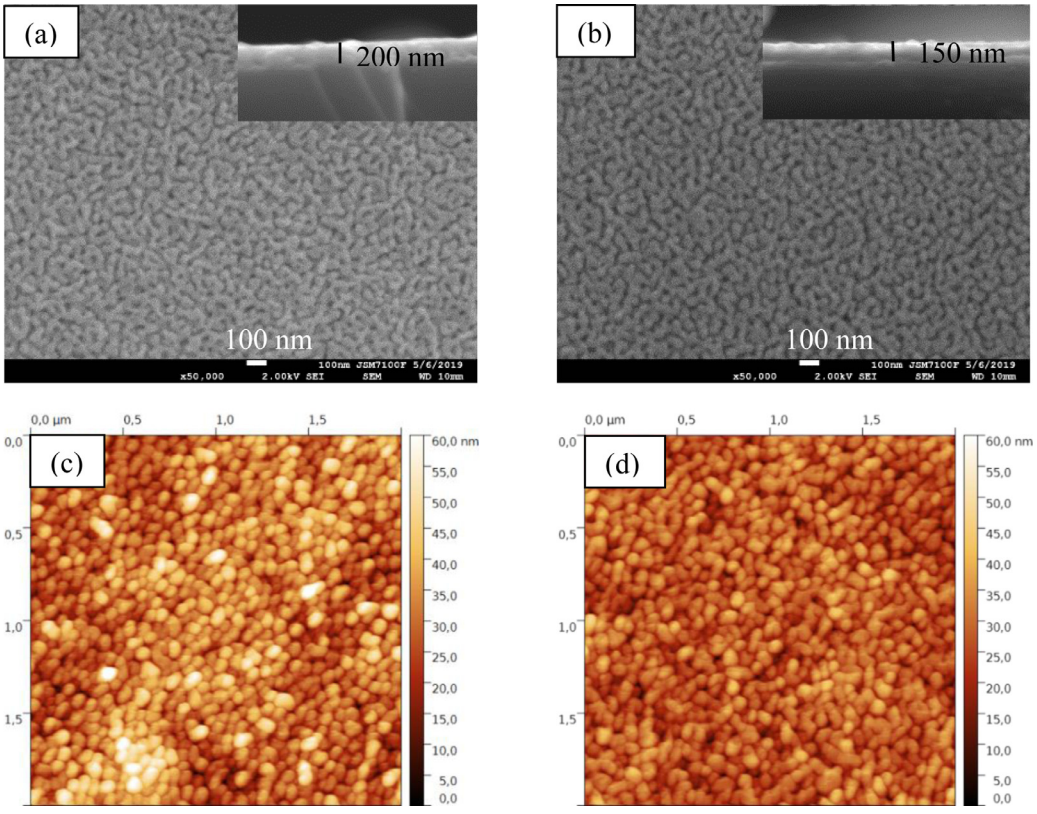

Fig 2. SEM and AFM images of BFO thin films synthesized at 500 °C on silica (a,c) and on (100)Si (b,d).

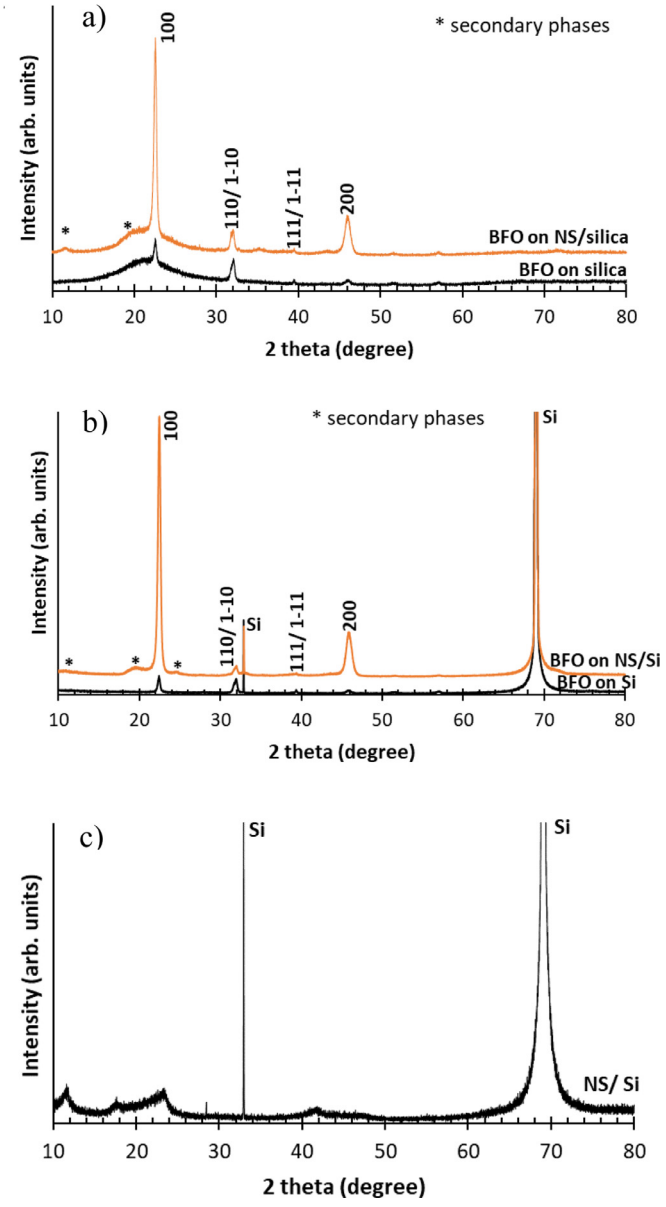

Fig 3. XRD patterns of BFO thin films synthesized at 500 °C on nanosheets (NS)/silica (a) and on nanosheets (NS)/(100)Si (b). Magnification of XRD pattern of nanosheets (NS)/ Si (c).

3.2. BFO thin films grown on nanosheets seed layers

Fig. 3a and 3b show the XRD patterns obtained for BFO films deposited on nanosheets/silica and on nanosheets/(100)Si respectively, and calcined at 500 °C-2 h. In contrast to the polycrystalline films directly deposited on silica and Si at this temperature, two intense peaks can be observed and indexed as (100) and (200) reflections of the distorted perovskite structure of BFO, which indicate clearly that the films deposited on nanosheets present a highly (100) oriented growth. The $Ca_2Nb_3O_{10}^-$ nanosheets have a perovskite-related structure with a 2D pseudo-square lattice of a close to 0.386 nm [1], which is close to the BFO lattice parameter (a = 0.3962 nm), giving a small lattice mismatch of +2.64%. Thus nanosheets seed layer can induce an oriented growth of BFO, synthesized by CSD, even on amorphous substrates or on substrates presenting structural incompatibilities. The mechanism of the film growth is a local epitaxy of the BFO phase on each nanosheet.

Nagasaka et al. [28] reported the preferential (100) growth of Mn-doped BFO films (300 nm thick) synthesized by CSD (using methoxyethanol solvent) at 500 °C on $Ca_2Nb_3O_{10}$ nanosheets layers previously deposited on (111)Pt/TiO_2/(100)Si and (111)Pt/ stainless steel substrates. In the case of platinized silicon substrate, the presence of the $Bi_2Fe_4O_9$ secondary phase was observed. Dral et al. [29] reported the epitaxial growth of a stack of $SrTiO_3$ (42 nm thick), $SrRuO_3$ (18 nm) and $BiFeO_3$ (20 nm) grown by pulsed laser deposition at 700 °C on $Ca_2Nb_3O_{10}^-$ nanosheets layers previously deposited on (001) phlogopite mica substrates. In our case, phi-scans XRD patterns (not shown here) performed with a 4-circle texture diffractometer revealed no in-plane preferential orientation of the BFO films. This result is not surprising since the nanosheets of several micrometers in lateral size are randomly turned on the substrates surface (Fig. 4).

On the XRD patterns of Fig. 3a and 3b, some other peaks of weak intensities can be observed that could be attributed to a reaction of the nanosheets with BFO and/or with the substrate leading to the formation of secondary phases, possibly $Bi_{5.96}Ca_{1.76}Nb_{0.28}O_{11.14}$ (JCPDS card No. 00-079-9855) for the peak located at 2θ = 19.8° However, it is quite difficult to confirm with certainty the composition of this phase with only one visible peak. H. Yan et al. [30] reported reaction of $Ti_{0.87}O_2$ nanosheet seeds with grown TiO_2. However, in their case, the reaction occurred because of the similar composition. The other observed extra peaks may correspond to the preferential orientation of a layered phase with a lattice constant equal to about c = 14.1–14.3 Å. In order to check if these last peaks may be associated to some of the nanosheets, XRD pattern was performed on a nanosheets layer deposited on Si. Magnification of this pattern (Fig. 3c) displays peaks corresponding to an inter-reticular distance of about 15.4 Å, in agreement with a previous study [31]. The shift of the extra peaks observed in the BFO films on nanosheets (from 15.4 to 14.1–14.3 Å) may correspond to the formation of a layered Bi/Si-$Ca_2Nb_3O_{10}$. Further investigations are underway to determine the exact composition of these secondary phases.

The TEM-EXDS analyses performed on the films confirmed the presence of Bi, Fe, O, Ca and Nb with a Bi/ Fe molar ratio equal to 1.

The SEM and AFM images of the films deposited on nanosheets seed layers on both substrates are displayed in Fig. 4. The films are relatively dense and homogeneous (Fig. 4a,b) with a uniform grain size around 80 nm (Fig. 4c,d) and present similar microstructures to those obtained for the films directly deposited on bare substrates. They have a thickness around 150 nm, as observed on the cross-sectional views (insets in Fig. 4a,b). Fig. 4e and 4f show the AFM images of the nanosheets deposited on silica and (100)Si by Langmuir–Blodgett process, before the BFO deposition. Nanosheets of several micrometers lateral size are clearly observed with a relatively good coverage on both substrates.

The TEM images performed on the BFO film deposited on nanosheets/(100)Si are displayed in Fig. 5. The in-plane view (Fig. 5a) revealed that the film is made of 50–100 nm wide crystals. Fig. 5b shows a [100] zone axis selected-area electron diffraction pattern of the film from an in plane-view specimen, in agreement with the preferential orientation observed by XRD. On the cross-sectional view (Fig 5c), the thickness of the 2 slabs of the film glued together is estimated to 640 nm, thus a film thickness of ~ 320 nm. Other areas observed by TEM (not shown) indicate local variations of film thickness from 150 to 400 nm. The BFO film is made of small grains and present some porosities.

Fig. 5d is a high magnification TEM micrograph of the cross-sectional sample, showing the morphology of the BFO film on the nanosheets/Si substrate. It can be observed the SiO_2 layer (in white) and above a layer with a continuous 6 nm thick layer. The secondary phase previously observed by XRD, possibly identified as $Bi_{5.96}Ca_{1.76}Nb_{0.28}O_{11.14}$, could be located in this 6 nm thick layer.

4. Conclusions

Single-phase BFO thin films were obtained at 400° − 500 °C by CSD using polymeric precursor method on bare amorphous silica and (100) Si substrates. These randomly oriented films present homogeneous

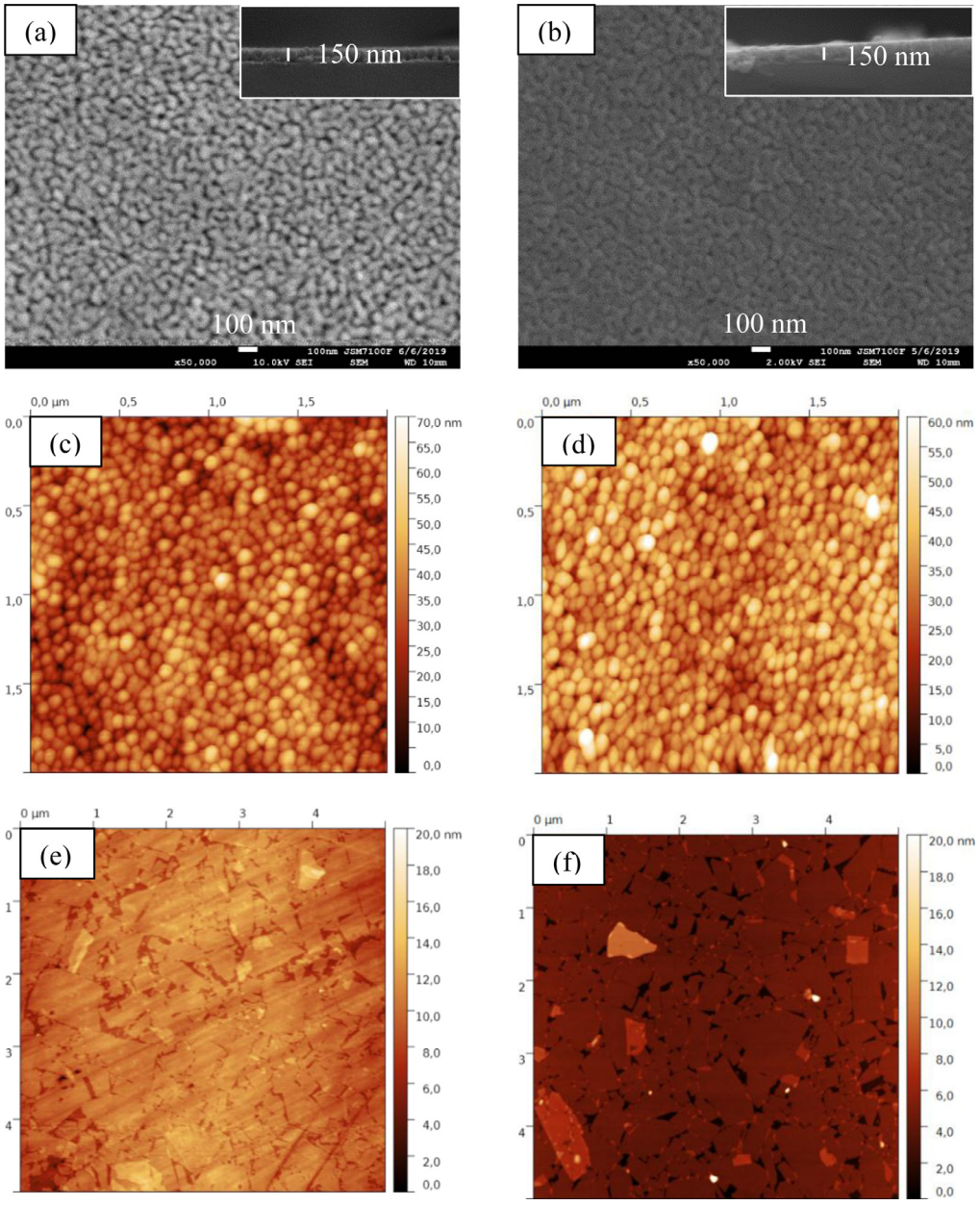

Fig 4. SEM and AFM images of BFO thin films synthesized at 500 °C on nanosheets/silica (a,c) and on nanosheets/(100) Si (b,d). AFM images of nanosheets (before BFO deposition) on silica (e) and on (100)Si (f).

microstructures with uniform grains size of 80 nm. The introduction of a nanosheets seed layer did not change the films microstructure but induced a highly oriented (100) growth of BFO on both substrates. However, secondary phases were observed that could be attributed to $Bi_{5.96}Ca_{1.76}Nb_{0.28}O_{11.14}$ and to a layered Bi/ Si-$Ca_2Nb_3O_{10}$ with a lattice constant equal to about c = 14.1–14.3 Ă. These results are nevertheless promising to provide a low-cost route for the integration of oriented BFO thin films in microelectronics. Indeed, the methods of synthesis for BFO thin films as well as for the nanosheets seed layer use low-cost precursors and simple equipment, and enable large area of deposition at low temperature on inexpensive substrates.

Declaration of Competing Interest

None

Acknowledgement

The authors thank the French “Agence Nationale de la Recherche” (ANR) in the framework of the POLYNASH project (ANR-17-CE08-0012). SEM and TEM experiments were performed on CMEBA and THEMIS platforms (ScanMAT, UMS 2001, University of Rennes 1-CNRS). ISCR and ScanMAT received a financial support from the Région Bretagne, Rennes Métropole, the Département d'Ille et Vilaine and the European Union (CPER-FEDER 2007–2014 and CPER 2015-2020 MULTIMAT ScanMAT).

Author Contributions Section

V. Bouquet: Investigation, Writing - original draft, Writing - review & editing, Visualization. F. Baudouin: Investigation, Writing - review & editing. V. Demange: Investigation, Writing - review & editing, Funding acquisition. S. Députier: Investigation, Writing - review & editing. S.

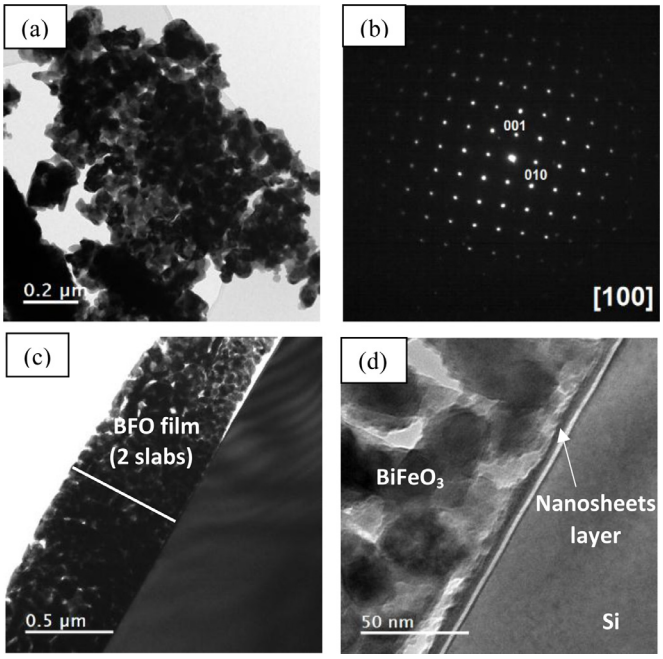

Fig 5. TEM micrographs of the BFO thin film synthesized at 500 °C on nanosheets/(100)Si: (a) in-plane view of the BFO film, (b) [100] zone axis electron diffraction pattern of a BFO film grain, (c,d) cross-sectional view of the sample at low and high magnification.

Ollivier: Investigation, L. Joanny: Investigation, L. Rault: Investigation, A. Fouchet: Project administration, Funding acquisition, Writing - review & editing. M. Guilloux-Viry: Investigation, Writing - review & editing.

References

[1] T. Shibata, K. Fukuda, Y. Ebina, T. Kogure, T. Sasaki, One-Nanometer-Thick seed layer of unilamellar nanosheets promotes oriented growth of oxide crystal films, Adv. Mater. 20 (2008) 231, https://doi.org/10.1002/adma.200701381.

[2] M. Nijland, S. Kumar, R. Lubbers, D.H.A. Blank, G. Rijnders, G. Koster, J.E. ten Elshof, Local control over nucleation of epitaxial thin films by seed layers of inorganic nanosheets, ACS Appl. Mater. Interfaces 6 (2014) 2777, https://doi.org/10.1021/am4052624 doi:dx.doi.org/.

[3] Y. Minemura, D. Ichinose, K. Nagasaka, J.W. Kim, H. Shima, K. Nishida, T. Kiguchi, T.J. Konno, N. Oshima, H. Funakubo, H. Uchida, Polar-axis-oriented crystal growth of tetragonal PZT films on stainless steel substrate using pseudo-perovskite nanosheet buffer layer, AIP Adv. 5 (2015) 77139, https://doi.org/10.1063/1.4927208 doi.org/.

[4] T. Shibata, H. Takano, Y. Ebina, D.S. Kim, T.C. Ozawa, K. Akatsuka, T. Ohnishi, K. Takada, T. Kogure, T. Sasaki, Versatile van der Waals epitaxy-like growth of crystal films using two-dimensional nanosheets as a seed layer: orientation tuning of $SrTiO_3$ films along three important axes on glass substrates, J. Mater. Chem. C 2 (2014) 441, https://doi.org/10.1039/c3tc31787k.

[5] K. Kikuta, K. Noda, S. Okumura, T. Yamaguchi, S i Hirano, Orientation control of perovskite thin films on glass substrates by the application of a seed layer prepared from oxide nanosheets, J. Sol-Gel Sci. Technol 42 (2007) 381, https://doi.org/10.1007/s10971-006-0200-z.

[6] M.D. Nguyen, H. Yuan, E.P. Houwman, M. Dekkers, G. Koster, J.E. ten Elshof, G. Rijnders, Highly oriented growth of piezoelectric thin films on silicon using two-dimensional nanosheets as growth template layer, ACS Appl. Mater. Interf. 82 (2016) 31120, https://doi.org/10.1021/acsami.6b09470.

[7] G. Catalan, J. Scott, Physics and applications of bismuth ferrite, Adv. Mater. 21 (2009) 2463, https://doi.org/10.1002/adma.200802849.

[8] D. Sando, A. Barthélémy, M. Bibes, $BiFeO_3$ epitaxial thin films and devices: past, present and future, J. Phys. Condens. Matter 26 (2014) 473201, , https://doi.org/10.1088/0953-8984/26/47/473201.

[9] T. Ahmed, A. Vorobiev, S. Gevorgian, Growth temperature dependent dielectric properties of $BiFeO_3$ thin films deposited on silica glass substrates, Thin Solid Films 520 (2012) 4470, https://doi.org/10.1016/j.tsf.2012.02.082.

[10] H.W. Chang, F.T. Yuan, S.H. Tien, C.Y. Shen, C.R. Wang, S.U Jen, Effect of substrates on the structure and ferroelectric properties of multiferroic $BiFeO_3$ films, IEEE Trans. Magn. 50 (No.1) (2014) 2500604, , https://doi.org/10.1109/TMAG.2013.2278702.

[11] N. Deepak, P. Carolan, L. Keeney, P.F. Zhang, M.E. Pemble, R.W. Whatmore, Bismuth self-limiting growth of ultrathin $BiFeO_3$ films, Chem. Mater. 27 (2015) 6508, https://doi.org/10.1021/acs.chemmater.5b03034.

[12] J. Thery, C. Dubourdieu, T. Baron, C. Ternon, H. Roussel, F. Pierre, MOCVD of $BiFeO_3$ thin films on $SrTiO_3$, Chem. Vap. Depos. 13 (2007) 232, https://doi.org/10.1002/cvde.200606571.

[13] G.A. Gomez-Iriarte, C Labre, L.A.S. de Oliveira, J.P Sinnecker, Pure phase $BiFeO_3$ thin films sputtered over Si: a new route towards high magnetization, J. Magn. Magn. Mater. 460 (2018) 83, https://doi.org/10.1016/j.jmmm.2018.03.056 doi.org/.

[14] M. Gaidi, N. Somrani, L. Stafford, In situ investigation of magnetron sputtering plasma used for the deposition of multiferroic $BiFeO_3$ thin films, J Mater. Sci. 28 (2017) 15749, https://doi.org/10.1007/s10854-017-7178-x.

[15] F. Tyholdt, S. Jørgensen, H. Fjellvåg, A.E. Gunnæs, Synthesis of oriented $BiFeO_3$ thin films by chemical solution deposition: phase, texture, and microstructural development, J. Mater. Res. 20 (2005) 2127, https://doi.org/10.1577/JMR.2005.0263.

[16] R.R. Awasthi, K. Asokan, B. Das, Effect of molar concentration on structural, magnetic domain and optical properties of $BiFeO_3$ thin films, Appl. Phys. A 125 (1) (2019) 338, https://doi.org/10.1007/s00339-019-2560-6 doi.org/.

[17] A.Z. Simões, A.H.M. Gonzalez, L.S. Cavalcante, C.S. Riccardi, E. Longo, J.A. Varela, Ferroelectric characteristics of $BiFeO_3$ thin films prepared via a simple chemical solution deposition, J. Appl. Phys. 101 (2007) 074108, , https://doi.org/10.1063/1.2715513 doi.org/.

[18] C.R. Foschini, M.A. Ramirez, S.R. Simoes, J.A. Varela, E. Longo, A.Z. Simoes, Piezoresponse force microscopy characterization of rare-earth doped $BiFeO_3$ thin films grown by the soft chemical method, Ceram. Int. 39 (2013) 2185, https://doi.org/10.1016/j.ceramint.2012.08.083 dx.doi.org/.

[19] I. Bretos, R. Jiménez, J. Ricote, M.L. Calzada, Low-temperature crystallization of solution derived metal oxide thin films assisted by chemical processes, Chem. Soc. Rev. 47 (2018) 291, https://doi.org/10.1039/c6cs00917d.

[20] M. Pechini, Method of preparing lead and alkaline-earth titanates and niobates and coating method using the same to form a capacitor, US Patent 3330697, 1967.

[21] Q. Simon, V. Bouquet, A. Perrin, M. Guilloux-Viry, Synthesis of $KTa_xNb_{1-x}O_3$ (KTN) powders and thin films by polymeric precursor method, Solid State Sci. 11 (2009) 91, https://doi.org/10.1016/j.solidstatesciences.2008.06.015.

[22] M.C.F. Alves, R.M.M. Marinho, G.P. Casali, M. Siu-Li, S. Députier, M. Guilloux-Viry, A.G. Souza, E. Longo, I.T. Weber, I.M.G. Santos, V. Bouquet, Influence of the network modifier on the characteristics of $MSnO_3$(M = Sr and Ca) thin films synthesized by chemical solution deposition, J. Solid State Chem. 199 (2013) 34, https://doi.org/10.1016/j.jssc.2012.11.014 doi.org/.

[23] A.L. Menezes de Oliveira, V. Bouquet, V. Dorcet, S. Ollivier, S. Députier, A.G. de Souza, M. Siu-Li, E. Longo, I.T. Weber, I.M.G. dos Santos, M. Guilloux-Viry, Evolution of the structural and microstructural characteristics of $SrSn_{1-x}Ti_xO_3$ thin films under the influence of the composition, the substrate and the deposition method, Surf. Coat. Technol. 313 (2017) 361, https://doi.org/10.1016/j.surfcoat.2017.01.082 dx.doi.org/.

[24] A.S. Maia, F. Cheviré, V. Demange, V. Bouquet, M. Pasturel, S. Députier, R. Lebullenger, M. Guilloux-Viry, F. Tessier, Preparation of niobium based oxynitride nanosheets by exfoliation of Ruddlesden-Popper phase precursor, Solid State Sci. 54 (2016) 17, https://doi.org/10.1016/j.solidstatesciences.2015.11.013 dx.doi.org/.

[25] M. Muramatsu, K. Akatsuka, Y. Ebina, K. Wang, T. Sasaki, T. Ishida, |.K. M.iyake, M. Haga, Fabrication of densely packed titania nanosheet films on solid surface by use of Langmuir－Blodgett deposition method without amphiphilic additives, Langmuir 21 (14) (2005) 6590, https://doi.org/10.1021/la050293f.

[26] H. Yuan, R. Lubbers, R. Besselink, M. Nijland, J.E. ten Elshof, Improved Langmuir–Blodgett titanate films via *in situ* exfoliation study and optimization of deposition parameters, ACS Appl. Mater. Interfaces 6 (2014) 8567, https://doi.org/10.1021/am501380d dx.doi.org/.

[27] H. Yuan, M. Timmerman, M. van de Putte, P. Gonzalez Rodriguez, S. Veldhuis, J.E. ten Elshof, Self-Assembly of metal oxide nanosheets at liquid-air interfaces in colloidal solutions, J. Phys. Chem. C 120 (2016) 25411, https://doi.org/10.1021/acs.jpcc.6b07961.

[28] K. Nagasaka, N. Oshima, J.W. KIM, H. Shima, A. Akama, T. Kiguchi, K. Nishida, T.J. Konno, H. Funakubo, H. Uchida, Fabrication of $(100)_c$-oriented Mn-doped bismuth ferrite films on silicon and stainless steel substrates using calcium niobate nanosheets, J. Ceram. Soc. Jpn. 123 (2015) 322, https://doi.org/10.2109/jcersj2.123.322 dx.doi.org/.

[29] A.P. Dral, M. Nijland, G. Koster, J.E. ten Elshof, Film transfer enabled by nanosheet seed layers on arbitrary sacrificial substrates, APL Mater. 3 (2015) 056102, , https://doi.org/10.1063/1.4921070 doi.org/.

[30] H. Yuan, K. Han, D. Dubbink, G. Mul, G, J.E. ten Elshof, Modulating the external facets of functional nanocrystals enabled by two-dimensional oxide crystal templates, ACS Catal. 7 (2017) 6858, https://doi.org/10.1021/acscatal.7b02605.

[31] B.-.W. Li, M. Osada, Y. Ebina, K. Akatsuka, K. Fukuda, T Sasaki, High thermal robustness of molecularly thin perovskite nanosheets and implications for superior dielectric properties, ACSNano 8 (2014) 5449, https://doi.org/10.1021/nn502014c.